arXiv:1609.06546v1 [astro-ph.SR] 21 Sep 2016

An Eruptive Hot-Channel Structure Observed at Metric Wavelength as a Moving Type-IV Solar Radio Burst

V. Vasanth[1], Yao Chen[1] †, Shiwei Feng[1], Suli Ma[2], Guohui Du[1], Hongqiang Song[1], Xiangliang Kong[1], and Bing Wang[1]

ABSTRACT

Hot channel (HC) structure, observed in the high-temperature passbands of the AIA/SDO, is regarded as one candidate of coronal flux rope which is an essential element of solar eruptions. Here we present the first radio imaging study of an HC structure in the metric wavelength. The associated radio emission manifests as a moving type-IV (t-IVm) burst. We show that the radio sources co-move outwards with the HC, indicating that the t-IV emitting energetic electrons are efficiently trapped within the structure. The t-IV sources at different frequencies present no considerable spatial dispersion during the early stage of the event, while the sources spread gradually along the eruptive HC structure at later stage with significant spatial dispersion. The t-IV bursts are characterized by a relatively-high brightness temperature ($\sim 10^7 - 10^9$ K), a moderate polarization, and a spectral shape that evolves considerably with time. This study demonstrates the possibility of imaging the eruptive HC structure at the metric wavelength and provides strong constraints on the t-IV emision mechanism, which, if understood, can be used to diagnose the essential parameters of the eruptive structure.

Subject headings: Sun: corona — Sun: activity — Sun: coronal mass ejections (CMEs) — Sun: radio radiation

1. Introduction

Hot channel (HC) structures, first observed through the high-temperature passbands at 131 and 94 Å of the Atmospheric Imaging Assembly (AIA: Lemen et al. 2012) on the Solar

[1]Institute of Space Sciences, Shandong University, Weihai, Shandong 264209, China yaochen@sdu.edu.cn, vasanth@sdu.edu.cn

[2]College of Science, China University of Petroleum, Qingdao 266580, China

Dynamic Observatory (SDO: Pesnell et al. 2012) (Cheng et al. 2011; Zhang et al. 2012), are regarded as one candidate of coronal flux ropes that are the main energy carrier and one of the essential elements of solar eruptions. It is not or hardly present in cooler passbands of AIA such as the 211 and 171 Å, indicating its temperature is as high as $5 - 10$ MK. The formation process and the associated heating mechanism of HCs, not resolved at this time, are likely related to some slow reconnections or volume current dissipations before or during the early stage of a flare. It is natural to further ask whether energetic electrons are also generated during the HC formation/heating and eruptive process and whether these energetic electrons can excite radio emissions. If yes, this may provide an additional observational window of the eruptive HC-flux rope structure, important to further diagnose its physical properties and explore its formation and eruptive mechanism, as well as the distribution of energetic electrons within the structure.

A latest study by Wu et al. (2016) shows that during the pre-impulsive stage the HC structure can be imaged in the microwave regime using the Nobeyama Radioheliograph (NoRH; Nakajima et al. 1994; Takano et al. 1997). They found that the HC at 17 GHz presents an overall-arcade like structure with several intensity enhancements bridged by relatively weak emission. Based on their analysis, the microwave emission within the HC is at least partly contributed to by non-thermal energetic electrons. The study thus presents a piece of observational evidence for the existence of non-thermal energetic electrons within the HCs. Here we continue to expand the radio imaging study on HC structures to the metric wavelength that presents a direct observational manifestation of energetic electrons in the inner corona.

It is well known that there exist five types of radio bursts at the metric wavelength, including type-I, II, III, IV, and V bursts (Wild & McCready 1950; Melrose 1980; McLean & Labrum, 1985). Among them, the type IV (t-IV) radio burst is the most likely type related to the eruptive flux rope structure, while the type I burst is related to active regions (ARs) often in the absence of strong solar activities, the type II burst is attributed to energetic electrons accelerated at coronal shocks (see Feng et al. 2013, 2015; Kong et al. 2012; Chen et al. 2014; Vasanth et al. 2014; Du et al. 2015 for latest studies), and type III and V bursts are given by energetic electrons accelerated at solar flares propagating outward along open field lines. The t-IV bursts are broadband continuum emission, further classified as the moving t-IV (t-IVm) and static t-IV bursts (Weiss 1963; Melrose, 1980), generally believed to be excited by energetic electrons trapped within certain magnetic structures, such as magnetic arches, loops, or plasmoid structures (Smerd & Dulk 1971; Vlahos et al. 1982; Stewart 1985). Different emitting mechanisms have been proposed, including the synchrotron and gyro-synchrotron emission (Boischot 1957; Bastian & Gray 1997; Bastian et al. 2001), the plasma emission (Duncan 1981; Stewart 1982; Ramesh et al. 2013), and the

electron cyclotron maser emission (Kujipers 1975; Lakhina & Buti 1985; Winglee & Dulk 1986).

Latest observational studies start to conduct combining analysis of the imaging data obtained by Nançay Radioheliograph (NRH; Kerdraon & Delouis 1997) at the metric wavelength (Tun & Voulidas 2013; Bain et al. 2014) and the high-quality EUV data given by SDO/AIA. Yet, due to the scarcity of events with a complete data set, till now only one t-IV event has been investigated along this line (Tun & Voulidas 2013; Bain et al. 2014). The two studies investigated the same t-IVm event and concluded that the gyro-cyclotron emission is responsible for the burst. This is based on the observational characteristics such as the relatively low brightness temperature ($T_B < 10^6$ K), the absence of spatial dispersion at different NRH imaging frequencies, and the power-law spectra typical for gyro-synchrotron emission. The radio sources are found to be co-spatial with an eruptive filament that may represent the core of the coronal mass ejection (CME).

Here we show another moving t-IV burst with properties distinct from those investigated by Tun & Voulidas (2013) and Bain et al. (2014). The burst is found to be closely associated with an eruptive HC structure, thus establishing the physical connection between the t-IV sources and the HC-flux rope, and demonstrating the possibility of imaging this essential component of solar eruptions at metric wavelength.

2. Overview of the Event: the HC eruption and the radio burst

The eruption originated in NOAA AR11429 at the northeastern limb on 2012 March 4. See Figure 1 (and the accompanying movie) for the AIA observed eruptive process at two hot passpands 131 and 94 Å and one cool passband 171 Å. This AR, well studied by a number of authors (e.g., Harker & Pevtsov 2013; Liu et al. 2014; Colaninno & Vourlidas 2015), is super-active releasing 15 M-class and 3 X-class flares and several CMEs during its transit across the disk from March 2 to March 17. The eruption studied here is associated with an M2-class flare located at N16E65 and a halo CME propagating at an average speed of 1306 km s^{-1} according to the Large Angle Spectroscopic Coronagraph (LASCO; Brueckner et al. 1995) C2 data. According to the GOES SXR light curves (see Figure 2a), the flare started at 10:29 UT and peaked at 10:52 UT lasting for nearly two hours.

The pre-eruption structure, clearly visible from the 94 Å image in the upper panels of Figure 1 (pointed at by a pair of red arrows), starts to rise slowly at ∼10:27 UT, several minutes before the flare start. The structure presents a highly curved morphology writhing around the main bright loops of the AR. It has one root at the northwestern side of the AR,

while the other root is unidentifiable and possibly located behind the AR. Along with its slow rise, the structure becomes clearly visible at 131 Å, yet remaining invisible at 171 Å. This indicates that the structure contains high-temperature plasmas.

Panels of Figure 1b present the eruptive structure. The original writhed structure evolves into a bright plasmoid connected to a co-moving faint arcade feature on its southern side that is clearly visible from the accompanying movie. The eruptive structure is best seen at 131 Å (and invisible at 171 Å), again indicating its high internal temperature. It represents an eruptive HC structure (Zhang et al. 2012), likely associated with a magnetic flux rope consisting of twisted field lines with free magnetic energy to power the subsequent solar eruption.

During the eruption, the HC gradually fades and becomes invisible around 10:45 UT, while at its northwestern foot there appears an obvious dimming region (see green arrows in Figure 1c). This indicates that the dimming is due to an evacuation of plasmas. The dimming region is surrounded by a narrow layer of brightenings that evolves dynamically, and expands slowly towards the northwestern direction during the eruption. The brightening layer is likely attributed to the dissipation of currents (or magnetic reconnection) at the interface of the HC and the surrounding magnetic field.

In Figure 2a, we also present the Fermi Gamma-ray Burst Monitor (GBM) (Meegan et al. 2009) data at three energy bands. This is to show the presence of HXR-emitting non-thermal electrons, as well as the timing of the flare. In Figure 2b-2c, we show distance-time maps along the slice S1 (see Figure 1b), which corresponds to the outward moving direction of the plasmoid of the HC. The overlying arcade that has been pushed outward by the HC (see black arrows in Figure 1) is clearly visible in the S1-171 Å map. The motion of the plasmoid can be separated into a slow rise stage at a speed of ~ 72 km s^{-1} and an eruptive stage at ~ 367 km s^{-1}, while the overlying 171 Å arcade expands at slightly smaller speeds of ~ 56 km s^{-1} and 335 km s^{-1} (along S1), according to the height measurements and linear fittings. This is in line with the suggestion that the eruption is driven by the HC structure.

On the other hand, the accompanying radio burst was recorded by the Artemis radio spectrograph (Kontogeorgos et al. 2006) and imaged by the NRH. From the spectra shown in Figure 3a, we see a wide-band continuum emission from ~ 200 to 20 MHz (10:38 to 11:00 UT). The spectra present a trend of downward drift with time. A data gap exists from $110 - 90$ MHz. It looks like that the radio burst continues after the gap till the frequency reaches the lower spectral end ($\sim$ 20-30 MHz).

The high frequency counterpart of the radio burst is not clear possibly due to the low sensitivity of the Artemis instrument as well as the strong radio interference. Yet, according

to the much more sensitive measurements of NRH, there exist weaker yet significant emissions from 150 to 445 MHz. From Figure 3, we see that the maximum intensity of these emissions is higher at lower frequencies, reaching $\sim$ 100 sfu at 445 MHz and $\sim$ 1200 sfu at 150 MHz. The burst at 445 MHz, the highest NRH observing frequency, starts around 10:34 UT, and lasts for $\sim$ 15 minutes. At lower NRH frequencies, the starting and peak times are delayed, and the duration becomes longer reaching $\sim$ 25 minutes for 150 MHz. This is in general consistent with the characteristics of a broadband emission that drifts towards lower frequency. Therefore, we conclude that the radio burst, starting from around 10:34 UT (at 445 MHz) and drifting to lower frequencies, represents a t-IVm event.

The temporal evolution of the polarization levels of the t-IVm burst is shown in Figures 3d and 3e, which are calculated as the ratio of the sum of Stokes-V over the sum of Stokes-I within the region defined by the contour level of 95 % of the maximum T_B in each NRH image. We see that the polarization levels vary significantly, being left-handed at earlier stage (before $\sim$ 10:42 UT), becoming right-handed and increasing gradually later, up to values $\sim$ 10-20% for 150 MHz and 50% for 327 MHz ($\sim$40% for 445 MHz) at $\sim$ 10:44 UT. The emission spectra given by the total flux intensities at different NRH frequencies are shown in Figure 3f during the t-IVm. The spectra are generally power-law like with an spectral index varying from -1 to -3. The spectral shape varies considerably with time.

The corresponding T_B images can be viewed from Figure 4 and the accompanying animation. The t-IVm sources can be identified through all NRH channels, consistent with the broadband continuum characteristic. The T_B maximum (T_{Bmax}) reaches higher values at lower frequencies, being $\sim 10^7$, 10^8, and 10^9 K at 432, 360, and 150 MHz, respectively. These high T_B values are important to further infer the emitting mechanism. From 10:39 to 10:43 UT the sources move outward (along with the plasmoid, see below). They disappear earlier and reach lower altitude at higher frequency. In general, lower frequency sources have higher T_B, consistent with the above description of the radio fluxes and the power-law like spectra. The NRH imaging data show a continuous motion and transition of radio sources from high to low frequencies, supporting the above conclusion that the t-IVm burst contains a high-frequency (200 - 445 MHz) component.

3. Correlation of the radio sources and the eruptive HC structure

In this section, we further examine the spatial correlation of the radio burst and the eruptive structure. To do this, in Figure 5 we plot the contour levels at 95% of T_{Bmax} at different frequencies of a certain time together, and superpose them onto the closest AIA 131 Å images. The sources can be roughly separated into two groups. The first group of

sources, at higher NRH frequencies (445 - 360 MHz), line up together on the northern side of the dimming HC foot region without considerable motion. This group does not belong to the t-IVm burst of study. The other group of sources, observable at almost all NRH frequencies, first move outward as a compact source without significant spatial dispersion and then get spatially dispersed. These sources correspond to the t-IVm burst of study.

According to the dynamical evolution and spatial correlation with the eruptive structure of the t-IVm related radio sources, we can separate the t-IVm event into two stages. In the first stage (see panels of Figure 5a, before $\sim$ 10:44 UT), the sources at different frequencies are largely co-spatial with the plasmoid, i.e., the top part of the HC, without obvious spatial dispersion as mentioned. In the second stage (Figure 5b, from $\sim$ 10:44 to 10:47 UT), the sources start to extend sunwards along the curved side arcade of the HC with considerable spatial dispersion. From the HC top part to its side arcade, the sources line up from high to low frequencies. For example, the 270 MHz source is still located at the top part while the lower frequencies shift sunward (in the projection plane). The projected distance between the 270 MHz and 150 MHz source centroids is about 120 arcsecs at 10:45 UT.

The height measurements of the 228 MHz sources along S1 have been over-plotted in Figure 2b with red vertical lines. The comparison with the plasmoid locations indicate the spatial coincidence between the HC plasmoid and the radio sources before 10:44 UT. Later, the sources get spatially dispersed and the HC structure becomes very faint and almost invisible. To reveal their spatial correlation, in the middle (10:45 UT) and right (10:46 UT) panels of Figure 5b we overlay the outline of the side arcade of the HC observed earlier at 10:40 UT (see Figure 5a). Assuming a propagation speed of 300 km s^{-1}, the eruptive structure can propagate a distance of 125 (150) arcsecs in 5 (6) minutes. It can be seen that the radio sources are consistent with the expected location and shape of the outward-propagating side arcade of the HC.

These observations indicate that the t-IVm sources are emitted by energetic electrons that are first trapped within the plasmoid structure and then get scattered along the expanding side-arcade structure of the eruptive HC.

Around 10:46 UT, the sources (360-270 MHz) start to appear at the southeastern side of the AR region. Later, more sources are present there and yield a nice formation, with lower frequency sources located at higher altitudes. The morphology of the formation is analogous to the leg of an open or a large-scale closed loop, pointing towards the AR or the dimming foot (see Figure 5c). For these radio sources, it is not possible to determine their spatial correlation with the eruptive HC structure which already becomes completely invisible in AIA images. This part of the burst should not be taken as a part of the t-IVm burst that shifts towards lower frequency. The radio emitting electrons, however, might be physically

related. For instance, the t-IVm emitting electrons may get dumped to the leg of the HC structure and continue to emit there when the confinement at the top and the flank fails. It is also possible that the radio burst is a part of the following decimetric flare continuum emission (see Figure 3a), and the energetic electrons are not related to those accounting for the t-IVm burst. Available data sets do not allow us to reach a conclusive statement.

4. Discussion

With the above analysis, we present strong evidence of the HC being the t-IVm emitting structure. According to the GBM data presented in Figure 2a at 27.3−50.9 keV, the HXR-emitting nonthermal electrons are present from 10:30 to 10:50 UT. During this interval, the plasmoid forms and erupts, likely a result of the flare reconnection, which may contain the most twisted magnetic field lines within the HC structure. This makes it an efficient trap of flare-injected energetic electrons, as inferred from the t-IVm sources being spatially correlated with the plasmoid at the earlier stage. Along with the upward eruption, the HC plasmoid may get untwisted to gradually release the confinement. This allows the electrons to spread over a larger section of the structure along its side arcade, as has been manifested by the spatially-dispersed radio sources in FIgure 5b.

Note that the CME structures have been imaged at the radio wavelength in earlier studies. Bastian et al. (2001) proposed the radio CME concept by investigating one specific event, in which the radio sources present an expanding loop shape. Later studies (Maia et al. 2007; Démoulin et al. 2012) present another event with similar characteristics, and claim that the radio sources correspond to the CME cavity. The sources in these two events are co-spatial at different frequencies, with a large spatial extension (several solar radii), a relatively low T_B ($\leq 10^6$ K), and a power-law spectra of radio fluxes. Based on these observations, they suggest that the bursts are given by the incoherent synchrotron emission mechanism. Similar observational characteristics are obtained for the latest imaging studies on a t-IVm burst combining the NRH and AIA data (Tun & Vourlidas 2013; Bain et al. 2014), as introduced earlier. They conclude that the t-IVm burst is given by the gyro-synchrotron emission.

Here we find very different characteristics. First, the radio sources at different frequencies are initially co-spatial with each other, yet later they spread across the emitting structure and get spatially dispersed with an organized pattern. Each source occupies a relatively small part, and together they delineate a larger section of the structure. The T_B is much higher than reported by those studies (consistent with some other earlier observations on the t-IVm radio bursts (Stewart et al. 1978; Duncan et al. 1980)). Therefore, we suggest that our event points to a different emitting mechanism, possibly a coherent one to

account for the high T_B. Since the radio bursts here are constrained to certain specific part of the HC, they should be attributed to energetic electrons trapped therein. This means that the classical plasma emission mechanism induced by fast electron beams propagating in background plasmas may not play a role here.

Another coherent emission mechanism that is associated with trapped electrons is the electron maser cyclotron emission, developed when electrons are lost from the trap to form a positive gradient of the velocity distribution function along the perpendicular direction in the velocity phase space (Wu et al. 1979). Earlier studies have used this mechanism to explain continuum radio bursts such as the t-IV burst (Winglee & Dulk 1986; Lakhina & Buti 1985). Yet, further studies are required to check whether this mechanism can properly account for the radio characteristics reported here.

Our study presents that the t-IVm sources are carried by the plasmoid-HC structure. Such structure is of high temperature, and not observable with earlier solar imaging instruments. It is therefore not known whether such structure is present in those earlier events.

The polarization data in our event present a change of handed sense. Since the polarization levels are strongly affected by the angle between the magnetic field and the wave vector, we tentatively attribute this observation to the presumed untwisting motion of the HC, which likely results in some rotation of the magnetic structure.

The last point of discussion is relevant to the ionospheric effect on source positions. Firstly, the significance of this effect declines with increasing frequency (Wild 1959; Bougeret 1981). At frequencies above 150 MHz the effect is generally small. Secondly, from the NRH movie accompanying Figure 4, the positional fluctuation of radio sources is not important in comparison to the overall motion of the sources, indicating that the effect of ionospheric irregularities is relatively weak. Lastly, in this event the radio sources, with an overall outward propagation, first concentrate around the plasmoid and then get scattered gradually along the HC side structure. This pattern is consistent with the eruption of the HC and not likely caused by the ionospheric effect, which tends to result in systematic position shift of sources at different frequencies. We therefore suggest that the ionospheric effect does not affect the result of this study.

5. Summary

This study demonstrates that the AIA-observed eruptive HC structure can be imaged with the NRH at various metric wavelengths in the form of a t-IVm burst. The radio sources at different frequencies are found to be co-spatial with the moving HC structure. Initially, the

sources are constrained at the plasmoid which is at the top front of the HC. Then, the sources at different frequencies spread across the structure to a larger region and line up across the HC side arcade. Other characteristics include a relatively-high brightness temperature ($\sim 10^7 - 10^9$ K), a moderate polarization with a change of the handed sense, and a power-law like spectral shape that evolves considerably with time. Preliminary discussion on the possible emitting mechanism has been presented, and more studies are required to further explore the diagnostic potential of this kind of events to infer the critical parameters/conditions of the eruptive structure.

We thank the Artemis, NRH, STEREO, SDO, and SOHO teams for providing the data. We also thank Dr. Koval and Dr. Hillaris for their help in plotting the dynamic spectrum. This work was supported by grants NNSFC 41274175, 41331068, and U1431103, and NSBRSF 2012CB825601.

REFERENCES

Bain, H. M., Krucker, S., Saint-Hilaire, P., et al. 2014, ApJ, 782, 43

Bastian, T. S., Pick, M., et al. 2001, ApJ, 558, L65

Bastain, T. S., and Gray, D. E. 1997, JGR, 102, 14031

Bougeret, J. L. 1981, A&A, 96, 259

Boischot, A. 1957, Compt. Rend. Acad. Sci. Prais, 244, 1326

Brueckner, G. E., Howard, R. A., Koomen, M. J., et al. 1995,SoPh,162, 357

Chen Y., Du G. H., Feng L. et al 2014, ApJ, 787, 59

Cheng, X., Zhang, J., Liu, Y., et al. 2011, ApJ, 732, L25

Colaninno R. C. and Vourlidas A. 2015, ApJ, 815, 70

Démoulin, P., Vourlidas, A., Pick, M., et al. 2012, ApJ, 750, 147

Du G. H., Kong X. L., Chen Y. et al 2015, ApJ, 812, 52

Duncan, R. A., Stewart, R. T., Nelson, G. J. 1980, in IAU symp. 91, 381

Duncan, R. A. 1981, SoPh, 73, 191

Feng S. W., Chen Y., Kong X. L. et al 2013, ApJ, 767, 29

Feng S. W., Du G. H., Chen Y. et al 2015, SoPh, 290, 1195

Harker B. J. and Pevtsov A. A. 2013, ApJ, 778, 175

Kong X. L., Chen Y., Li G. et al 2012, ApJ, 750, 158

Kontogeorgos, A., Tsitsipis, P., Caroubalos, C., et al. 2006, ExA, 21, 41

Kuijpers, J.: 1975, Solar Phys. 44, 173

Lakhina, G. S. and Buti, B. 1985, SoPh, 99, 277

Lemen, J. R., Title, A. M., Akin, D. J., et al. 2012, SoPh, 275, 17

Liu Y. T., Richardson J. D., Wang C., et al. 2014, ApJL, 788, L28

Low, B. C., Hundhausen, J. R. 1995, ApJ, 443, 818

Maia, D. J. F., Gama, R., Mercier, C. et al. 2007, ApJ, 660, 874

Meegan, C., Lichti, G., Bhat, P. N., et al. 2009, ApJ, 702, 791

Melrose D. B. 1980 SSRv, 26, 3

Nakajima, H., Nishio, M., Enome, S., et al. 1994, IEEEP, 82, 705

Nelson, G.J., Melrose, D.B. 1985, In: McLean, D.J., Labrum, N.R. (eds.) Solar Radiophysics, Cambridge University Press, Cambridge, 37.

Parker, E. N. 1957, JGR, 62, 509

Pesnell, W. D., Thompson, B. J., Chamberlin, P. C., et al. 2012, SoPh, 275, 3

Priest, E., Forbes, T. 2000, Cambridge University press, New york

Ramesh, R., Kishore, P., Mulay, S. M., et al. 2013, ApJ, 778, 30

Smerd, S. F. and Dulk, G. A. 1971, IAU Symp. 43, Solar Magnetic Fields, ed. R. Howard (Dordrecht: Reidel), 616

Stewart, R. T., Duncan, R. A., Suzuki, S., et al. 1978, Proc. Astron. Soc. Australia, 3, 247

Stewart, R. T. 1985, in Solar Radio Physics, Cambridge University press, 361

Sweet, P. A. 1958, IAUS, 6, 123S

Takano, T., Nakajima, H., Enome, S., et al. 1997, LNP, 483, 183

Tun, S. D., and Vourlidas, A. 2013, ApJ, 766, 130

Vasanth V., Umapathy S., Vrnak B. et al 2014, SoPh, 289, 251

Vlahos, L., Gergely, T. E., and Papadopoulos, K. 1982, ApJ, 258, 812

Weiss, A. A. 1963, AuJPh, 16, 526

Wild, J. P., Sheridan, K. V., & Neylan, A. A. 1959, AuJPh, 12, 369

Wild, J.P., McCready, L.L. 1950, Aust. J. Sci. Res., Ser. A 3, 387

Winglee, R. M.; Dulk, G. A. 1986, ApJ, 307, 808

Wu C. S. and Lee L. C. 1979, ApJ, 230, 621

Wu, Z., Chen, Y., Huang, G., et al. 2016, ApJL, 820, L29

Zhang, J., Cheng, X., Ding, M. D., et al. 2012, Nat. commun., 3, 747

This preprint was prepared with the AAS LaTeX macros v5.2.

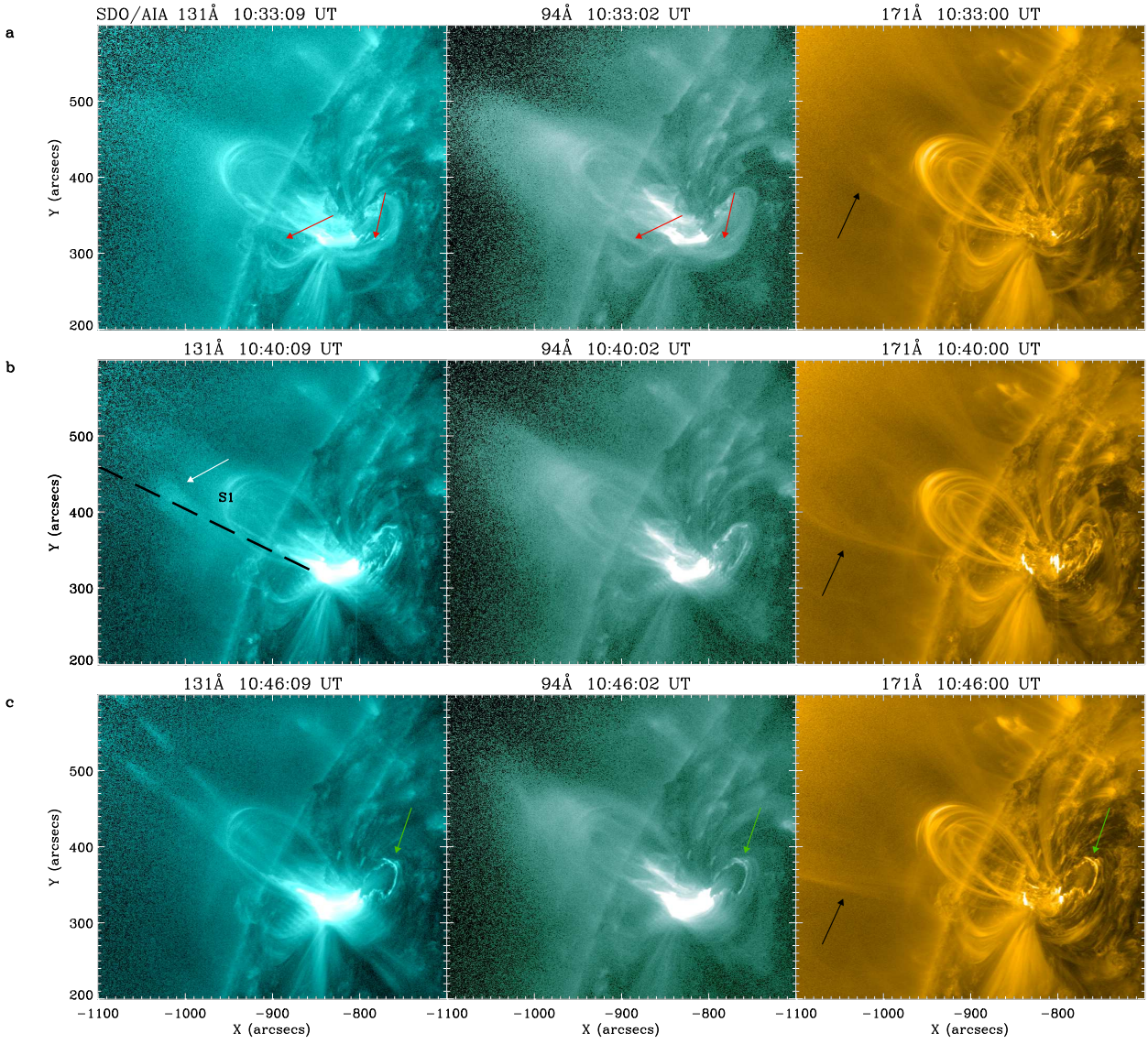

Fig. 1.— The HC eruption recorded by AIA at 131, 94, and 171 Å at (a) 10:33 UT (to show the slowly rising HC, red arrows), (b) 10:40 UT (to show the eruptive plasmoid-HC structure, white arrows), and (c) 10:46 UT (to show the dimming foot region, green arrows). S1 is for the distance maps shown in Figure 2. An accompanying movie of both direct and base difference images is available online.

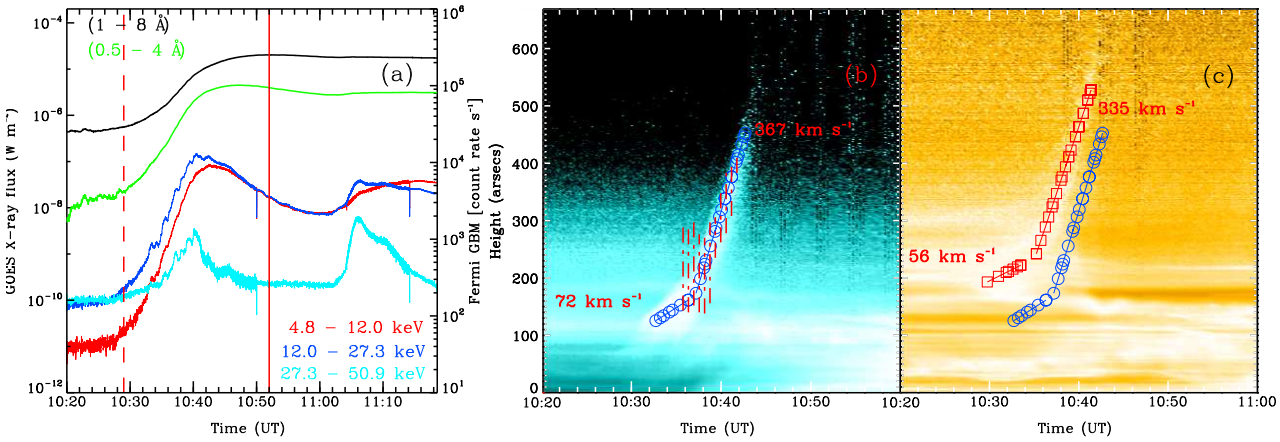

Fig. 2.— (a) The GOES SXR light curves (1-8 Å, and 0.5-4 Å) and the Fermi GBM data (detector n2) at 4.8-12.0, 12.0-27.3, and 27.3-50.9 keV. The GBM data have been averaged at a time resolution of 2 s. The direction angle of the n2 detector to the Sun is stable and around 60 degrees during the time of interest (10:30-11:00 UT). The two vertical lines indicate the flare start (10:29) and peak (10:52) time. (b-c) Distance-time maps along the slice S1 observed at AIA 131 and 171 Å. The velocities are given by linear fitting. Red vertical lines in panel (b) represent the NRH source positions given by the 95% T_{Bmax} contour levels at 228 MHz.

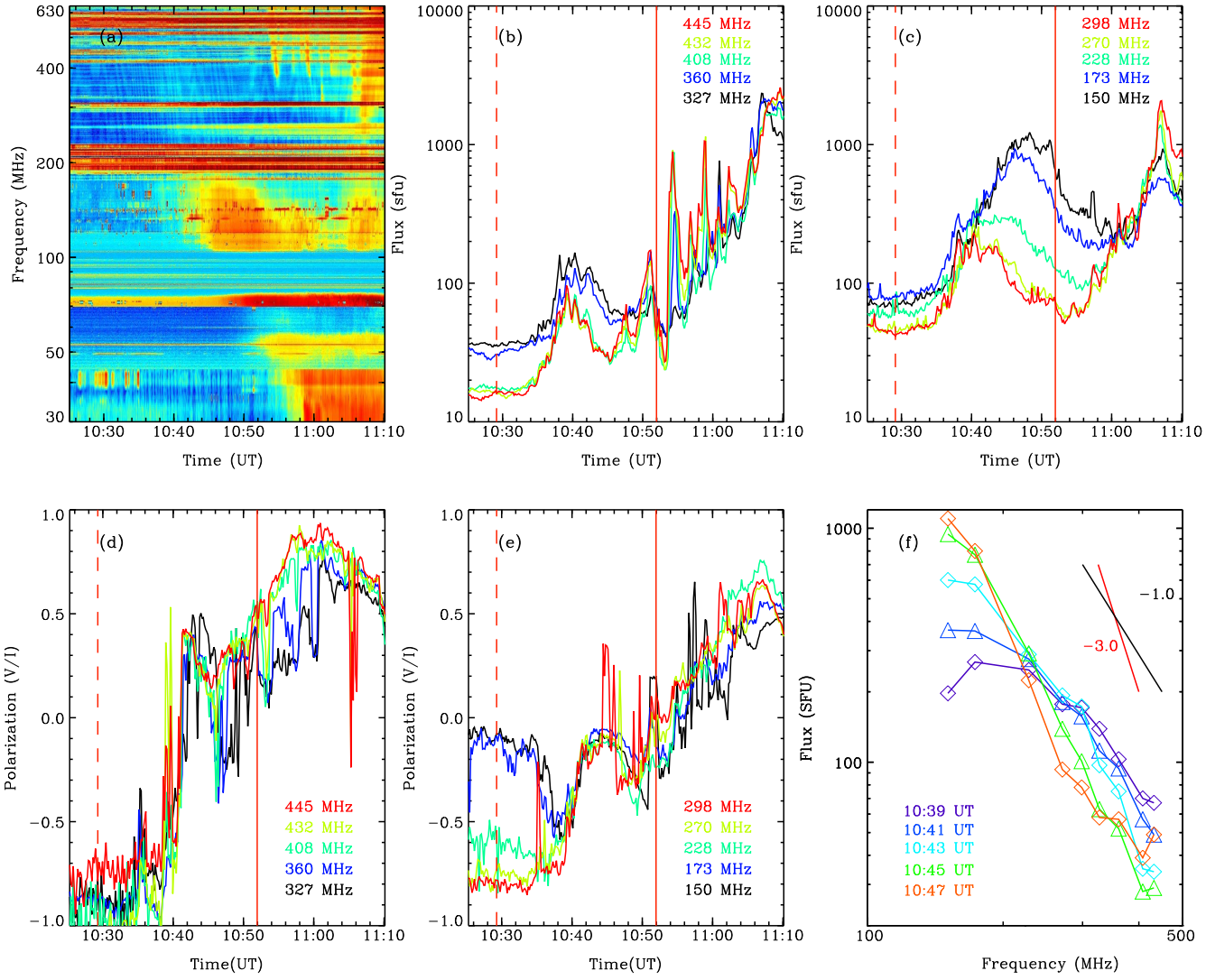

Fig. 3.— Characteristics of the t-IVm burst as recorded by Artemis and NRH. (a) the Artemis dynamic spectrum; (b-c) total NRH fluxes and (d-e) polarization levels; (f) the emission spectra at selected moments. The two vertical lines indicate the flare start and peak time.

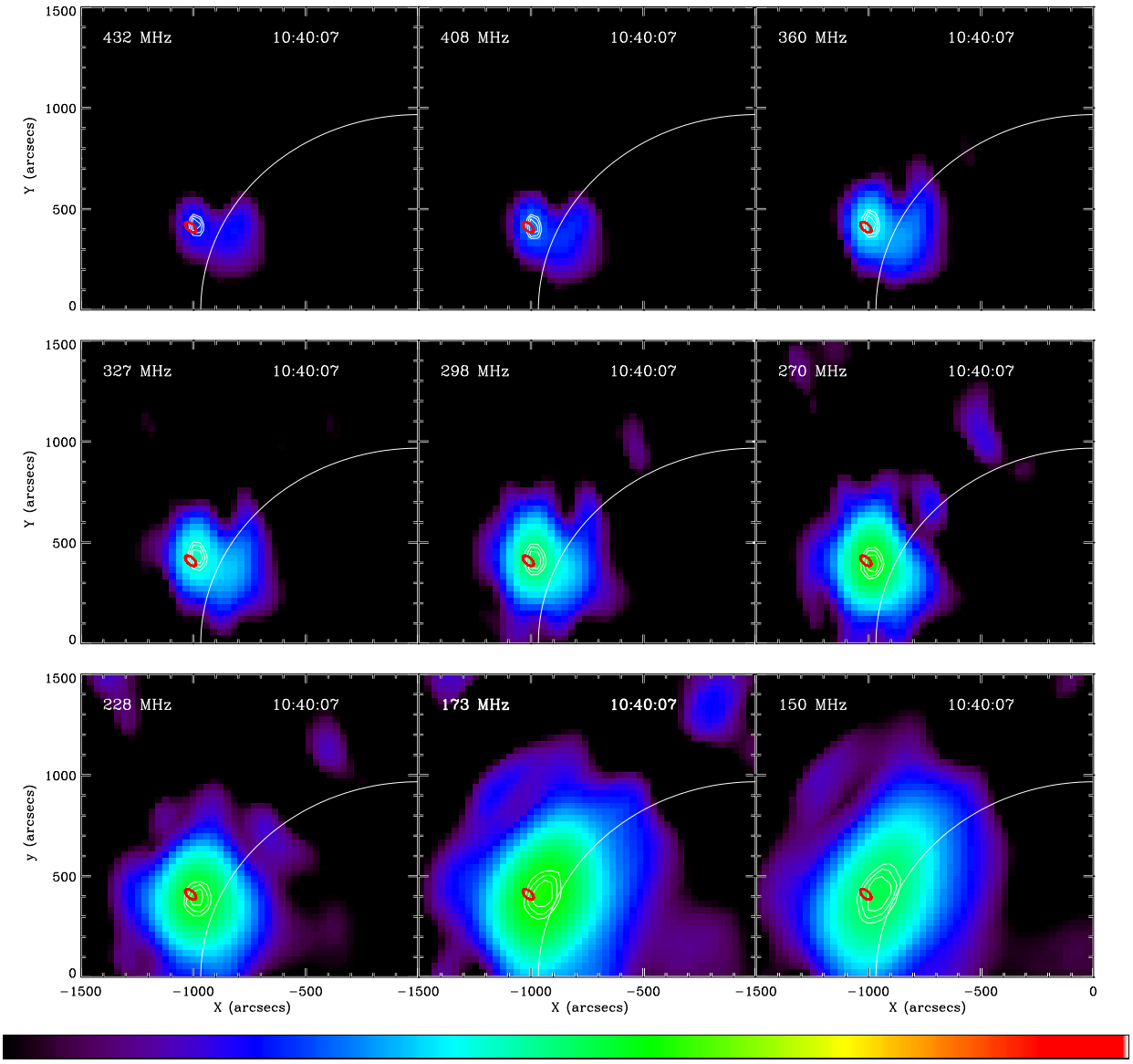

Fig. 4.— NRH images at different frequencies at 10:40 UT. The contour levels represent 85 %, 90 %, and 95 % of T_{Bmax}. The location of the HC-plasmoid observed by AIA at the same time is denoted with a red ellipse. An accompanying movie is available online.

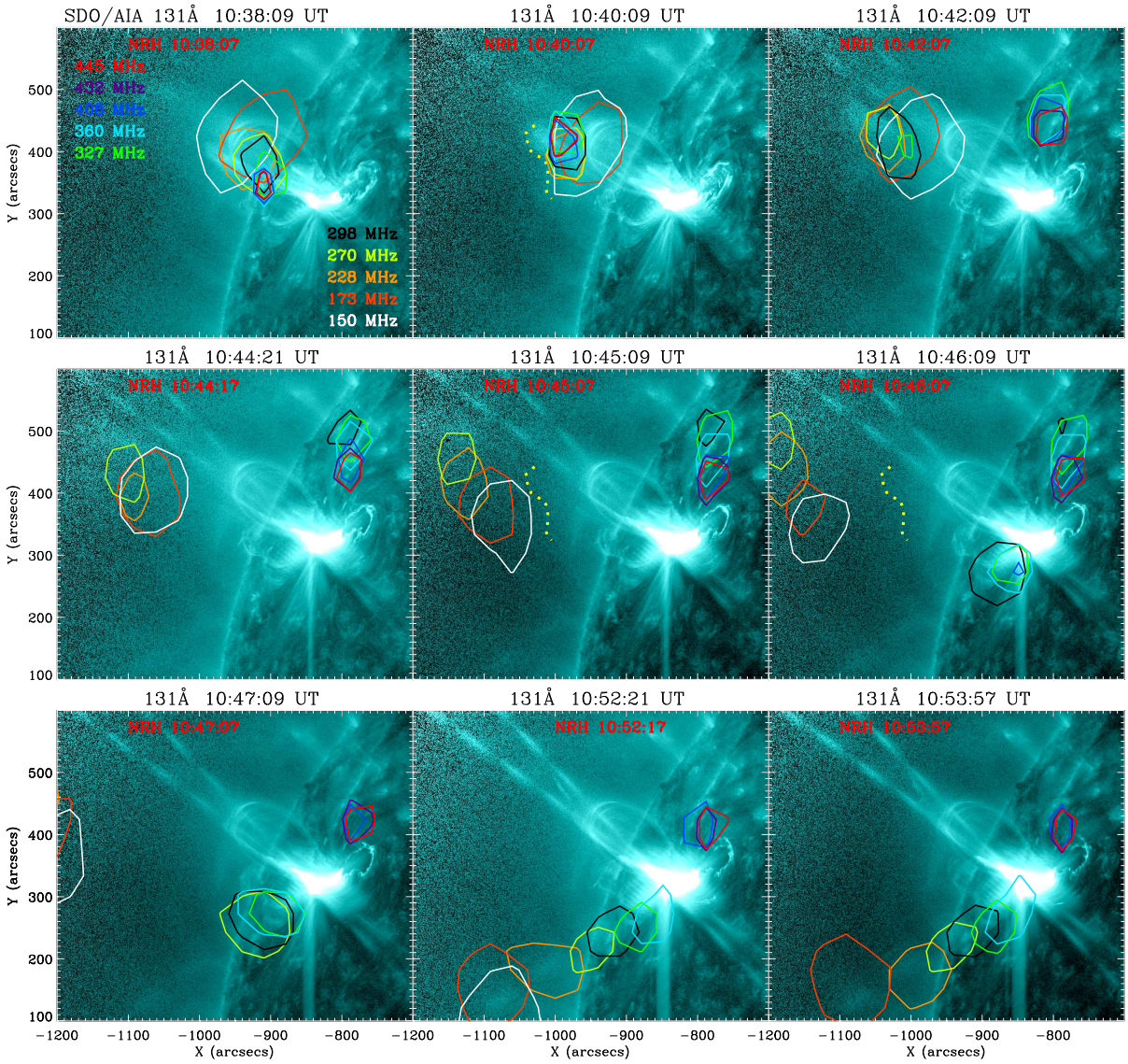

Fig. 5.— (a-c) Temporal evolution of the NRH sources, superposed onto the closest-in-time AIA 131 Å images. The NRH data are represented by the 95% T_{Bmax} contours. The yellow dotted lines present the outline of the side arcade inferred at 10:40 UT. An accompanying movie (with AIA difference images) is available online.